

ORIGINAL ARTICLE

Chirality-induced antisymmetry in magnetic domain wall speed

Dae-Yun Kim¹, Min-Ho Park¹, Yong-Keun Park^{1,2}, Joo-Sung Kim¹, Yune-Seok Nam¹, Duck-Ho Kim^{1,3}, Soong-Geun Je^{1,4}, Hyeok-Cheol Choi¹, Byoung-Chul Min² and Sug-Bong Choe¹

In chiral magnetic materials, numerous intriguing phenomena such as built-in chiral magnetic domain walls (DWs) and skyrmions are generated by the Dzyaloshinskii–Moriya interaction (DMI). The DMI also results in asymmetric DW speeds under an in-plane magnetic field, which provides a useful scheme to measure the strength of the DMI. However, recent findings of additional asymmetries such as chiral damping have inhibited the unambiguous determination of the DMI strength, and the underlying mechanism of overall asymmetries comes under debate. Here, we experimentally investigate the nature of the additional asymmetry by extracting the DMI-induced symmetric contribution from the DW speed. Our results reveal that the additional asymmetry has a truly antisymmetric nature with the typical behavior governed by the DW chirality. In addition, the antisymmetric contribution alters the DW speed by a factor of 100, dominating the overall variation in DW speed. Thus, experimental inaccuracies can be largely removed by calibration with such antisymmetric contributions, enabling the standard DMI measurement scheme.

NPG Asia Materials (2018) 10, e464; doi:10.1038/am.2017.216; published online 19 January 2018

INTRODUCTION

Understanding magnetic domain wall (DW) motion is of extreme importance owing to its potential application in spintronic devices such as memory and logic devices.^{1–4} In order to improve the performance of these devices, it is crucial to achieve fast DW speeds. It has been reported that fast DW speeds can be achieved with intrinsic chiral DWs⁵ generated by the Dzyaloshinskii–Moriya interaction (DMI),^{6,7} where the DMI is an antisymmetric exchange interaction originating from structural inversion asymmetries.^{8,9} In the case of skyrmion-based devices, the DMI also determines the stability of the skyrmion (that is, the ability of the device to store data). Therefore, the precise measurement and control of the DMI are crucial in designing DW-mediated spintronic devices. Various experimental techniques have been proposed to quantify the DMI.^{10–15} Among them, one of the simplest techniques is a symmetry measurement of the DW's speed with respect to an in-plane magnetic field.¹⁰ In this technique, the shift of the symmetric axis indicates the magnitude of the DMI-induced effective magnetic field directly. However, many other groups have subsequently reported the existence of an additional asymmetry, which makes it difficult to unambiguously determine the symmetric axis. In this regard, the investigation of the additional asymmetry is important not only from an academic viewpoint, but also to ensure an error-free DMI measurement technique. Quite recently, several

possible mechanisms^{16–21} were proposed for the additional asymmetry, but their validity remains under debate. Here, we have experimentally demonstrated the chiral nature of the additional asymmetry. By extracting the well-known DMI-induced symmetric contribution from the DW's motion, the additional asymmetry is found to exhibit a truly antisymmetric nature, which is governed by the DW's chirality.

MATERIALS AND METHODS

For this study, four different Ta/Pt/Co/X/Pt films, where X = Al, Pt, Ti or W, were deposited on Si substrates with a 100-nm-thick SiO₂ oxide layer by DC magnetron sputtering. The detailed layer structures were 5.0-nm Ta/2.5-nm Pt/0.9-nm Co/2.5-nm X/1.5-nm Pt for X = Al, Ti or W, and 5.0-nm Ta/2.5-nm Pt/0.5-nm Co/1.5-nm Pt for X = Pt, where the upper Pt layer was employed as the protection layer.²² Magnetic wire structures with a width of 20 μm and length of 500 μm were then patterned on the films using a photolithography technique. All the magnetic wires exhibited strong perpendicular magnetic anisotropy and showed clear domain expansion under the application of an out-of-plane magnetic field H_z . The DW images were recorded using a magneto-optical Kerr effect microscope equipped with both out-of-plane and in-plane electromagnets, which could apply a magnetic field of up to 40 and 200 mT on the sample, respectively. All the images in our present work were taken at a magnification of $\times 200$ with an optical spatial resolution of $\sim 1 \mu\text{m}$, where the width of each CCD pixel corresponded to $\sim 0.8 \mu\text{m}$ on the sample surface. The DW speed v_{DW} was then measured by analyzing successive domain images captured with a constant time interval under application of H_z , as

¹Department of Physics and Institute of Applied Physics, Seoul National University, Seoul, Republic of Korea and ²Center for Spintronics, Korea Institute of Science and Technology, Seoul, Republic of Korea

³Present address: Institute for Chemical Research, Kyoto University, 611-0011 Kyoto, Japan.

⁴Present address: SPINTEC, CEA/CNRS, 38054 Grenoble, France.

Correspondence: Professor S-B Choe, Department of Physics and Astronomy, Seoul National University 1 Gwanak-ro, Room #410, Building #23, Gwanak-gu, Seoul 08826, Republic of Korea.

E-mail: sugbhong@snu.ac.kr

Received 7 April 2017; revised 17 October 2017; accepted 24 October 2017

exemplified by Figure 1a and Supplementary Figure S1. This measurement procedure was repeated under application of various current densities, J , and/or an in-plane magnetic field H_x bias.

Figure 1b shows a plot of ν_{DW} with respect to H_z for positive and negative current densities, that is, $+J$ (blue) and $-J$ (red). It is clear that the two curves exhibit the same behavior except for the shifts along the abscissa axis, where the direction of the shift is determined by the polarity of the current bias. When the two curves are shifted by $\pm \Delta H_{\text{eff}}$ along the abscissa axis, they overlap onto a single curve (black open circles). According to Franken *et al.*,²³ ΔH_{eff} is a direct measure of the effective magnetic field caused by the current bias, and yields the relation $\Delta H_{\text{eff}} = \varepsilon_{\text{ST}} J$, where ε_{ST} is defined as the spin-torque efficiency for the current-to-field conversion.²⁴ On the basis of the above-mentioned relation, the ε_{ST} of our samples was determined from the measurement of ΔH_{eff} with respect to J . In our experiments, these measurements were obtained for $|J| < 1 \times 10^{10} \text{ A m}^{-2}$, for which the associated temperature rise due to Joule heating was negligible ($< 0.5 \text{ K}$).²⁵

RESULTS

In Figure 2a, ε_{ST} is plotted with respect to H_x for one of our X=Al samples (for the other samples, Supplementary Figure S2). The figure shows the typical spin-orbit-torque-induced behavior composed of three regimes: the two saturation regimes (NW \pm regimes) separated by a transient regime (that is, the Bloch-Néel wall (BW-NW) regime).^{26,27} In the NW \pm regimes, the DW is saturated to the Néel-type configuration, where the magnetization inside the DW is oriented along the $\pm x$ axes. On the other hand, in the BW-NW regime, the DW varies between the Bloch- and Néel-type configurations. The x intercept (red vertical line) indicates the magnetic field H_0 required to achieve the Bloch-type DW configuration. In order to achieve such a configuration, H_0 should exactly compensate the DMI-induced effective magnetic field H_{DMI} , that is, $H_0 + H_{\text{DMI}} = 0$. Therefore, H_{DMI}

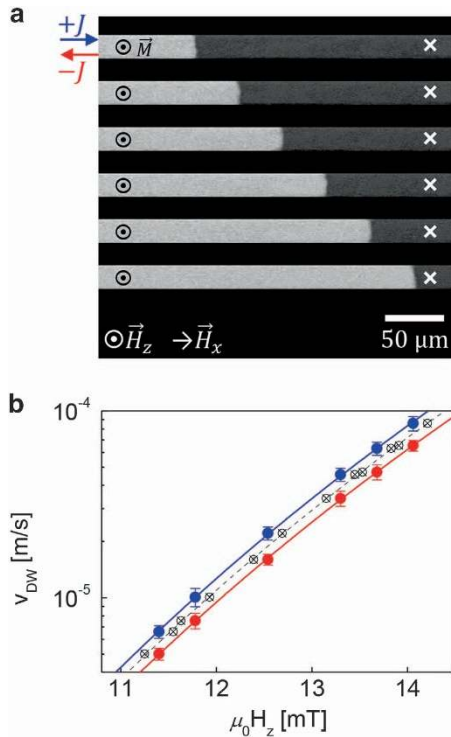


Figure 1 (a) Successive DW images under application of H_z with a constant time interval (1 s). The directions of H_z , H_x , J , and the magnetization M are as indicated. (b) Plot of ν_{DW} with respect to H_z for opposite current biases: $+J$ (blue) and $-J$ (red). The black open symbols represent the data for $\pm J$ after shifting the values along the abscissa by $\pm \Delta H_{\text{eff}}$, respectively.

can be quantified from the x intercept of the magnetic field measurements. For this sample, H_{DMI} was estimated as $-107 \pm 8 \text{ mT}$, where the accuracy of the H_{DMI} measurement is governed by the statistics of the determination of $\varepsilon_{\text{ST}}(H_x)$ and the accuracy of H_x . The corresponding magnitude of the DMI is finally determined as $D = 0.87 \pm 0.08 \text{ mJ m}^{-2}$ (Supplementary Table S1).

Next, the variation in the DW speed under the application of a constant out-of-plane magnetic field H_z with an in-plane magnetic field bias H_x was measured. Figure 2b shows ν_{DW} with respect to H_x for three different H_z biases. The orange, green and blue symbols present the data for $H_z = 8.6, 9.9$ and 11.0 mT , respectively. In contrast to the symmetric behavior reported by Je *et al.*,¹⁰ the present sample exhibited highly asymmetric behavior. Samples with such large asymmetry need to be analyzed carefully because the field H_0^* (blue vertical line) corresponding to the minimum ν_{DW} occurs far from H_0 .

Recent studies^{10,16–21} have shown that DW motion follows the DW creep criticality, as given by $\nu_{\text{DW}}(H_x) = \nu_0 \exp[-\alpha(H_x)H_z^{-1/4}]$, where ν_0 is the characteristic speed and $\alpha(H_x)$ is a scaling parameter related to the energy barrier. Here, $\alpha(H_x)$ has its maximum value for a Bloch-type DW configuration and shows symmetric variation with respect to H_x around the maximum. Recalling that the Bloch-type configuration is achieved for $H_x = H_0$, one can decompose the symmetric contribution S with respect to the axis $H_x = H_0$ into the form

$$S(\Delta H_x) \equiv \frac{1}{2} [\ln\{\nu_{\text{DW}}(H_0 + \Delta H_x)\} + \ln\{\nu_{\text{DW}}(H_0 - \Delta H_x)\}], \quad (1)$$

where ΔH_x is the deviation of H_x from H_0 (that is, $\Delta H_x \equiv H_x - H_0$). The symbols in Figure 2c show S plotted as a function of ΔH_x for three different values of the H_z bias.

Then, using Equation (6) from Je *et al.*,¹⁰ α can be written as

$$\alpha(H_0 + \Delta H_x) = \begin{cases} \alpha(H_0) \left[1 + \frac{2K_D \lambda}{\sigma_0} - \frac{\pi \lambda M_S}{\sigma_0} |\Delta H_x| \right]^{1/4} & \text{NW}^\pm \text{ regimes} \\ \alpha(H_0) \left[1 - \frac{\pi^2 \lambda M_S^2}{8K_D \sigma_0} (\Delta H_x)^2 \right]^{1/4} & \text{BW - NW regime} \end{cases}, \quad (2)$$

where λ is the DW width, M_S is the saturation magnetization, K_D is the DW anisotropy and σ_0 is the Bloch-type DW energy density. Using the well-known relations $\lambda = \sqrt{A/K_{\text{eff}}}$ and $\sigma_0 = 4\sqrt{AK_{\text{eff}}}$, where A is the exchange stiffness and K_{eff} is the uniaxial magnetic anisotropy, along with the definitions of the effective anisotropy field $H_K = 2K_{\text{eff}}/M_S$ and DW saturation field $H_S = 4K_D/\pi M_S$, Equation (2) can be written as

$$\alpha(H_0 + \Delta H_x) = \begin{cases} \alpha(H_0) \left[1 - \frac{\pi}{4H_K} (2|\Delta H_x| - H_S) \right]^{1/4} & \text{for } |\Delta H_x| > H_S \\ \alpha(H_0) \left[1 - \frac{\pi}{4H_K H_S} (\Delta H_x)^2 \right]^{1/4} & \text{otherwise} \end{cases}, \quad (3)$$

where the Néel-type configuration in the NW \pm regimes is achieved under the condition that $|\Delta H_x| > H_S$.

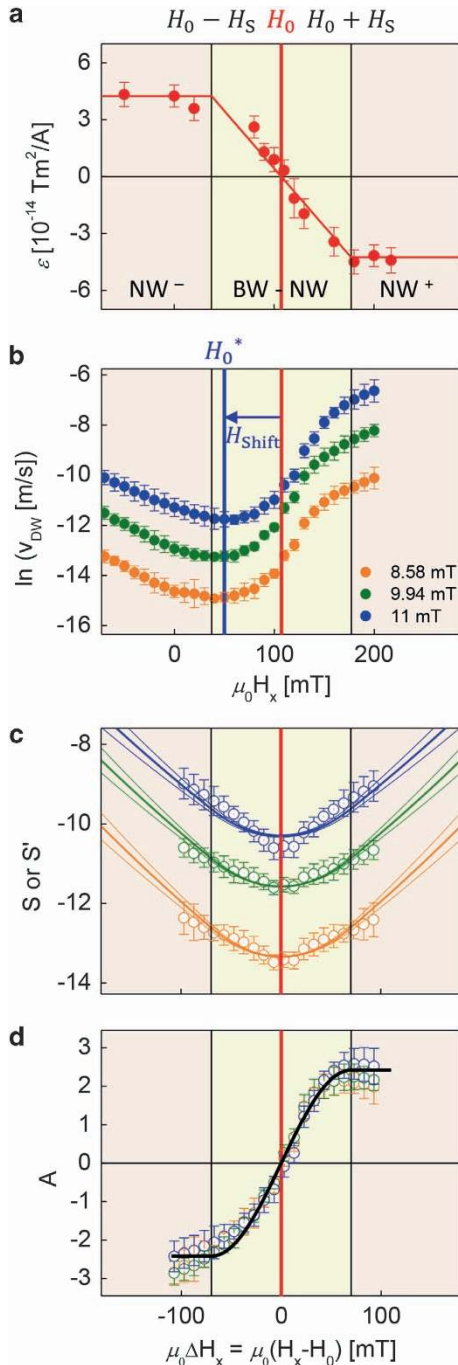
As Equation (3) is expressed using even functions of ΔH_x , the variation in α results in the symmetric contribution S' with respect to ΔH_x being given by

$$S'(\Delta H_x) \equiv \ln\{\nu_0(H_0)\} - \alpha(H_0 + \Delta H_x) H_z^{-1/4}. \quad (4)$$

Thus, as all the parameters in Eqs. (3) and (4) can be determined by independent measurements, we can therefore evaluate $S'(\Delta H_x)$, as shown by the solid line in Fig. 2c. The values ν_0 ($H_0 = 2.92 \times 10^{15} \text{ m/s}$) and $\alpha_0 = 14.9 \text{ T}^{1/4}$ were determined by the measurement of the creep criticality. The value of $H_K = 0.94 \text{ T}$ was determined using a vibrating sample magnetometer, while $H_S = 70 \text{ mT}$

was determined from Fig. 2a. It is interesting to note that $S'(\Delta H_x)$ exactly overlaps onto $S(\Delta H_x)$, even without any fitting parameter being used for these two curves. This observation implies that the symmetric contribution to the DW speed can be mostly attributed to the variation of α , which is known to be caused by the variation of the DW's energy density.

The additional asymmetry A is then resolved by subtracting the symmetric contribution S' from the DW speed v_{DW} (that is, $A \equiv \ln v_{\text{DW}} - S'$). Figure 2d shows A with respect to ΔH_x , where the solid line is a guide to the eye. It is clearly seen from the plot that the additional asymmetry has a truly antisymmetric nature (Supplementary Figure S5). Please note that this antisymmetric nature is generally observed for the other Xs (Supplementary Figure S3).



DISCUSSION

It is worthwhile to note that the antisymmetric contribution exhibits similar behavior to that of the ε_{ST} measurement (Figure 2a), with three regimes composed of a transition regime (BW-NW regime) in-between two saturation regimes (NW[±] regimes). As the DW chirality governs such typical regimes, one can conclude that the antisymmetric nature of A can be mainly attributed to the DW chirality. Such antisymmetry is possibly attributed to either the variation in v_0 via the chiral damping mechanism^{17,18} or to an additional variation of α arising from the intrinsic asymmetry of the variation in the DW's width.¹⁹ We are presently unable to distinguish the exact contributions from these variations (for details, please see Supplementary Section 6), but the antisymmetric nature can be further analyzed as follows.

As shown in Figure 2b, because of the significant antisymmetric contribution, the minimum value of v_{DW} occurs at a value of H_0^* , which is shifted from the position of H_0 . This apparent value of H_0^* is often misinterpreted as a compensation field of H_{DMI} . We have denoted the magnitude of the shift by H_{shift} (blue horizontal arrow) in Figure 2b. As the antisymmetric contribution saturates at H_S , it is natural to expect that $H_{\text{shift}} < H_S$. In addition, H_{shift} should be close to the value of H_S because the antisymmetric contribution leads to the magnitude of v_{DW} being increased by a factor of 100, dominating over the symmetric contribution in the BW-NW transition regime (Supplementary Figure S4). To demonstrate this prediction, H_{shift} was measured for all samples (that is, those with different X layers) and plotted with respect to H_S , as shown by Figure 3. The solid black line ($H_{\text{shift}} = H_S$) represents the upper bound of H_{shift} . This observation proves that the experimental inaccuracy in the $v_{\text{DW}}(H_x)$ -based DMI measurement does not exceed a few tens of mT (that is, the inaccuracy of the H_S measurement), which might be acceptable for measurement of a large DMI. It is also worthwhile to note that the sign of H_{shift} is uniquely determined by the DW chirality, and that a large portion of the experimental inaccuracy can therefore be removed by calibrating the measurement of H_S . In Figure 3, the inaccuracy remains less than ~ 10 mT. Finally, we note that H_S can also be estimated by $H_S \approx 2 \ln 2 \mu_0 M_S t_f / \pi^2 \lambda$, where t_f is the thickness of the magnetic layer.²⁸

In summary, we have examined the nature of the additional asymmetric contribution in the variation of a DW's speed. The symmetric contribution to the DW speed is well explained in terms of the DW's energy density. The additional asymmetry has a truly antisymmetric nature, which is possibly attributed to the DW's chirality. By improving our understanding of the nature of antisymmetric

Figure 2 (a) Plot of ε_{ST} with respect to H_x . The red vertical line indicates the value of H_0 by the x intercept. The NW[±] and BW-NW regimes are shown using different shaded areas, of which the boundaries are shown by the black vertical lines lying $\pm H_S$ from H_0 . (b) Plot of $\ln v_{\text{DW}}$ with respect to H_x for three different values of H_z . The orange, green and blue symbols represent data for $H_z = 8.6, 9.9$ and 11.0 mT, respectively. The error bars indicate the s.d. of repeated v_{DW} measurements (20 repetitions). The blue vertical line indicates the value of H_0^* for the minimum v_{DW} and the blue horizontal arrow shows H_{shift} . (c) Plot of S (symbols) and S' (solid lines) with respect to ΔH_x . The dashed lines show the possible error in the S' determination. The error bars δS were calculated by the addition of the statistical errors in the two measurements of $\ln v_{\text{DW}}$, that is, $\delta S = \frac{1}{2} \sqrt{(\delta \ln v_{\text{DW}1})^2 + (\delta \ln v_{\text{DW}2})^2}$, where $S = \frac{1}{2} [\ln v_{\text{DW}1} + \ln v_{\text{DW}2}]$. (d) Plot of A (symbols) with respect to ΔH_x . The solid line is a guide to the eye used to highlight the antisymmetry. The error bars δA were calculated by the statistical addition of the errors of $\ln v_{\text{DW}}$ and S' values, that is, $\delta A = \sqrt{(\delta \ln v_{\text{DW}})^2 + (\delta S')^2}$, where $A = \ln v_{\text{DW}} - S'$.

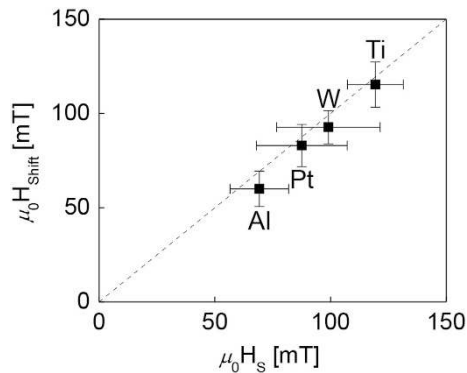


Figure 3 Plot of H_{shift} with respect to H_S . The black solid line ($H_{\text{shift}} = H_0$) represents the upper bound of H_{shift} for each layer material X. The error bars δH_S were calculated using the s.d. of all the possible fitting values of H_S for several different sets of $\varepsilon_{\text{ST}}(H_x)$. The error bars δH_{shift} were calculated by the statistical addition of δH_0 and δH_0^* , that is, $\delta H_{\text{shift}} = ([\delta(H_0)]^2 + [\delta(H_0^*)]^2)^{1/2}$, where H_{shift} is defined as $H_{\text{shift}} = H_0 - H_0^*$.

contribution, it is possible to remove a large portion of the experimental inaccuracy present in DMI measurements based on the DW's speed asymmetry. The present work provides an error-free DMI measurement technique that enables one to unambiguously measure the DMI, in addition to investigating the origin of the additional asymmetry.

CONFLICT OF INTEREST

The authors declare no conflict of interest.

ACKNOWLEDGEMENTS

This work was supported by grants from the National Research Foundation of Korea (NRF), funded by the Ministry of Science, ICT and Future Planning of Korea (MSIP; 2015R1A2A1A05001698 and 2015M3D1A1070465). Y-KP and B-CM were supported by the National Research Council of Science and Technology (NST; Grant No. CAP-16-01-KIST) by the Korean government (MSIP). D-HK was supported as an Overseas Researcher by a Postdoctoral Fellowship of the Japan Society for the Promotion of Science (Grant No. P16314).

Author contributions: D-YK and D-HK planned and designed the experiment, and S-BC supervised the study. D-YK, J-SK and Y-SN performed the measurements. M-HP, Y-KP, H-CC and B-CM prepared the samples. S-BC, D-YK, D-HK and S-GJ performed the analysis and wrote the manuscript. All authors discussed the results and commented on the manuscript.

PUBLISHER'S NOTE

Springer Nature remains neutral with regard to jurisdictional claims in published maps and institutional affiliations.

- Parkin, S. S. P., Hayashi, M. & Thomas, L. Magnetic domain-wall racetrack memory. *Science* **320**, 190 (2008).
- Moon, K.-W., Kim, D.-H., Yoo, S.-C., Je, S.-G., Chun, B.-S., Kim, W.-D., Min, B.-C., Hwang, C.-Y. & Choe, S.-B. Magnetic bubblecade memory based on chiral domain walls. *Sci. Rep.* **5**, 9166 (2015).
- Allwood, D. A., Xiong, G., Faulkner, C. C., Atkinson, D., Petit, D. & Cowburn, R. P. Magnetic domain-wall logic. *Science* **309**, 1688–1692 (2005).
- Hayashi, M., Thomas, L., Moriya, R., Rettner, C. & Parkin, S. S. P. Current-controlled magnetic domain-wall nanowire shift register. *Science* **320**, 209–211 (2008).
- Emori, S., Bauer, U., Ahn, S.-M., Martinez, E. & Beach, G. S. D. Current-driven dynamics of chiral ferromagnetic domain walls. *Nat. Mater.* **12**, 611 (2013).
- Thiaville, A., Rohart, S., Jué, E., Cros, V. & Fert, A. Dynamics of Dzyaloshinskii domain walls in ultrathin magnetic films. *Europhys. Lett.* **100**, 57002 (2012).

- Heide, M., Bihlmayer, G. & Blügel, S. Dzyaloshinskii-Moriya interaction accounting for the orientation of magnetic domains in ultrathin films: Fe/W(110). *Phys. Rev. B* **78**, 140403(R) (2008).
- Dzyaloshinsky, I. A thermodynamic theory of "weak" ferromagnetism of antiferromagnetics. *J. Phys. Chem. Solids* **4**, 241–255 (1958).
- Moriya, T. Anisotropic superexchange interaction and weak ferromagnetism. *Phys. Rev.* **120**, 91 (1960).
- Je, S.-G., Kim, D.-H., Yoo, S.-C., Min, B.-C., Lee, K.-J. & Choe, S.-B. Asymmetric magnetic domain-wall motion by the Dzyaloshinskii-Moriya interaction. *Phys. Rev. B* **88**, 214401 (2013).
- Ryu, K.-S., Thomas, L., Yang, S.-H. & Parkin, S. Chiral spin torque at magnetic domain walls. *Nat. Nanotechnol.* **8**, 527 (2013).
- Hrabec, A., Porter, N. A., Wells, A., Benitez, M. J., Burnell, G., McVitie, S., McGrouther, D., Moore, T. A. & Marrows, C. H. Measuring and tailoring the Dzyaloshinskii-Moriya interaction in perpendicularly magnetized thin films. *Phys. Rev. B* **90**, 020402(R) (2014).
- Cho, J., Kim, N.-H., Lee, S., Kim, J.-S., Lavrijsen, R., Solignac, A., Yin, Y., Han, D.-S., van Hoof, N. J. J., Swagten, H. J. M., Koopmans, B. & You, C.-Y. Thickness dependence of the interfacial Dzyaloshinskii-Moriya interaction in inversion symmetry broken systems. *Nat. Commun.* **6**, 7635 (2015).
- Han, D.-S., Kim, N.-H., Kim, J.-S., Yin, Y., Koo, J.-W., Cho, J., Lee, S., Klaui, M., Swagten, H. J. M., Koopmans, B. & You, C.-Y. Asymmetric hysteresis for probing Dzyaloshinskii-Moriya interaction. *Nano Lett.* **16**, 4438 (2016).
- Kim, D.-H., Yoo, S.-C., Kim, D.-Y., Min, B.-C. & Choe, S.-B. Wide-range probing of Dzyaloshinskii-Moriya interaction. *Sci. Rep.* **7**, 45498 (2017).
- Lavrijsen, R., Hartmann, D. M. F., van den Brink, A., Yin, Y., Barcones, B., Duine, R. A., Verheijen, M. A., Swagten, H. J. M. & Koopmans, B. Asymmetric magnetic bubble expansion under in-plane field in Pt/Co/Pt: effect of interface engineering. *Phys. Rev. B* **91**, 104414 (2015).
- Jué, E., Safeer, C. K., Drouard, M., Lopez, A., Balint, P., Buda-Prejbeanu, L., Bouille, O., Auffret, S., Schuhl, A., Manchon, A., Miron, I. M. & Gaudin, G. Chiral damping of magnetic domain walls. *Nat. Mater.* **15**, 272 (2016).
- Akosa, C. A., Miron, I. M., Gaudin, G. & Manchon, A. Phenomenology of chiral damping in noncentrosymmetric magnets. *Phys. Rev. B* **93**, 214419 (2016).
- Kim, D.-Y., Kim, D.-H. & Choe, S.-B. Intrinsic asymmetry in chiral domain walls due to the Dzyaloshinskii-Moriya interaction. *Appl. Phys. Express* **9**, 053001 (2016).
- Lau, D., Sundar, V., Zhu, J.-G. & Sokalski, V. Energetic molding of chiral magnetic bubbles. *Phys. Rev. B* **94**, 060401(R) (2016).
- Kim, D.-H., Yoo, S.-C., Kim, D.-Y., Min, B.-C. & Choe, S.-B. Universality of Dzyaloshinskii-Moriya interaction effect over domain-wall creep and flow regimes. *arXiv* **1608**, 01762 (2016).
- Park, Y.-K., Kim, D.-Y., Kim, J.-S., Nam, Y.-S., Park, M.-H., Min, B.-C. & Choe, S.-B. Empirical correlation between the interfacial Dzyaloshinskii-Moriya interaction and work function in metallic magnetic trilayers. *arXiv* **1710**, 06588 (2017).
- Franken, J. H., Herps, M., Swagten, H. J. M. & Koopmans, B. Tunable chiral spin texture in magnetic domain-walls. *Sci. Rep.* **4**, 5248 (2014).
- Lee, J.-C., Kim, K.-J., Ryu, J., Moon, K.-W., Yun, S.-J., Gim, G.-H., Lee, K.-S., Shin, K.-H., Lee, H.-W. & Choe, S.-B. Universality classes of magnetic domain wall motion. *Phys. Rev. Lett.* **107**, 067201 (2011).
- Kim, D.-H., Moon, K.-W., Yoo, S.-C., Min, B.-C., Shin, K.-H. & Choe, S.-B. A method for compensating the Joule-heating effects in current-induced domain wall motion. *IEEE Trans. Magn.* **49**, 3207 (2013).
- Haazen, P. P. J., Murè, E., Franken, J. H., Lavrijsen, R., Swagten, H. J. M. & Koopmans, B. Domain wall depinning governed by the spin Hall effect. *Nat. Mater.* **12**, 299 (2013).
- Je, S.-G., Yoo, S.-C., Kim, J.-S., Moon, J., Min, B.-C. & Choe, S.-B. Emergence of huge negative spin-transfer torque in atomically thin Co layers. *Phys. Rev. Lett.* **118**, 167205 (2017).
- Jung, S.-W., Kim, W., Lee, T.-D., Lee, K.-J. & Lee, H.-W. Current-induced domain wall motion in a nanowire with perpendicular magnetic anisotropy. *Appl. Phys. Lett.* **92**, 202508 (2008).



This work is licensed under a Creative Commons Attribution 4.0 International License. The images or other third party material in this article are included in the article's Creative Commons license, unless indicated otherwise in the credit line; if the material is not included under the Creative Commons license, users will need to obtain permission from the license holder to reproduce the material. To view a copy of this license, visit <http://creativecommons.org/licenses/by/4.0/>

© The Author(s) 2018

Supplementary Information accompanies the paper on the NPG Asia Materials website (<http://www.nature.com/am>)